Published in J. Electron. Mater. 29 (2000) 1122-1236

Experimental and Thermodynamic Assessment of Sn-Ag-Cu Solder Alloys

K.-W. Moon, W. J. Boettinger, U. R. Kattner, F. S. Biancaniello, and C. A. Handwerker

Metallurgy Division
Materials Science and Engineering Laboratory
NIST
Gaithersburg, MD 20899
USA

Abstract

Sn-rich alloys in the Sn-Ag-Cu system are being studied for their potential as Pb-free solders. Thus, the location of the ternary eutectic involving L, (Sn), Ag_3Sn and Cu_6Sn_5 phases is of critical interest. Phase diagram data in the Sn-rich corner of the Sn-Ag-Cu system are measured. The ternary eutectic is confirmed to be at a composition of 3.5 wt % Ag, 0.9 wt % Cu at a temperature of 217.2 ± 0.2 °C (2σ). A thermodynamic calculation of the Sn-rich part of the diagram from the three constituent binary systems and the available ternary data using the CALPHAD method is conducted. The best fit to the experimental data is 3.66 wt % Ag and 0.91 wt % Cu at a temperature of 216.3 °C. Using the thermodynamic description to obtain the enthalpy- temperature relation, the DTA signal is simulated and used to explain the difficulty of liquidus measurements in these alloys.

Key Words: Pb-free solder, Sn-Ag-Cu solder, phase diagram, ternary eutectic, and thermal analysis.

Introduction

Ternary alloys based on Sn-rich Sn-Cu and Sn-Ag binary eutectics have attracted considerable attention as potential Pb-free solders. The National Center for Manufacturing Science report [1] on Pb-free alloys showed that these binaries as well as their combinations have favorable solderability and wetting properties. It is important to have a rather precise knowledge of the phase diagram in order to optimize solder compositions for industrial trials because the levels of Cu and Ag in these solders are quite small (typically 3.5 wt % Ag and 1 wt % Cu). In particular, a Pb-free task group of the National Electronic Manufacturing Initiative [2] has focused on these alloys for manufacturing and reliability testing.

In 1959, Gebhardt and Petzow [3] presented a liquidus surface for the entire ternary. Based on very little data, they proposed a transition reaction, L + $Cu_6Sn_5 \rightarrow (Sn)^*$ + Ag_3Sn at 225 °C with a liquid composition of 4.0 wt % Ag, 0.5 wt % Cu. In 1960, Fedorov et al. [4] presented three isopleths, where a ternary eutectic reaction at 218 °C is evident in the Sn-rich corner. In 1994, Miller et al. [5], using DTA, found a ternary eutectic at 217 °C and placed its composition at 4.7 wt % Ag, 1.7 wt % Cu. A patent was issued based on this work [6]. Most recently, Loomans and Fine [7] place the ternary eutectic composition at 3.5 wt % Ag and 0.9 wt % Cu using thermal analysis of the signal from the monovariant binary eutectics, L→ (Sn) + Cu_6Sn_5 and L → (Sn) + Ag_3Sn.

---

* The symbol, (Sn), will be used to designate the Sn phase in contrast to the component Sn.

Using thermal analysis, the present work has examined alloys along two isopleths in the vicinity of the reported ternary eutectic compositions. These results and other selected data are used to develop a thermodynamic model for the Sn-rich portion of the ternary phase diagram. The difficulty of liquidus measurement for the intermetallics in this system is discussed using simulated DTA curves. These DTA curves are based on the calculated enthalpy-temperature predictions of the thermodynamic model.

Experimental Procedures

Preliminary thermodynamic calculations performed by one of the authors (URK), and reported* by Miller et al. [5] predicted a ternary eutectic and indicated that the Cu_6Sn_5 and Ag_3Sn liquidus surfaces were quite steep compared to the (Sn) liquidus. This can also be easily seen from the two binary diagrams. Thus, it was important to perform thermal analysis at sufficiently high temperatures to access the entire melting interval. In addition, simple lever law calculations indicated that the amount of primary intermetallic in the composition range of interest is quite small (≈ 2 wt %). Thus the liquidus signal during thermal analysis was likely to be weak; therefore, special attention was paid to the sensitivity of the thermal analysis technique.

Small alloy ingots were prepared by melting 99.99% purity metals in sealed and evacuated quartz ampoules at 1100 °C followed by agitation and water quenching. The chosen compositions lie along two sections, A and B, as shown in Fig.1. Section A was chosen to study the liquidus surfaces of Cu_6Sn_5 and Ag_3Sn. Section B was chosen to include the ternary eutectic composition reported by Loomans and Fine [7]. Elemental weights are considered accurate to approximately 0.1 mg producing very small composition errors.

For thermal analysis, 2 g samples were cut longitudinally from each ingot to minimize any macrosegregation effects and were re-melted in a test tube in air at approx. 250 °C. A fine 250 μm Inconel* sheathed chromel-alumel thermocouple was inserted in the center of the melt. The interior of the test tube and the thermocouple were coated with boron nitride. This coating was found to reduce, but not eliminate, the tendency for the liquid to supercool with respect to the (Sn) phase. The thermocouple was held in place by a glass test tube stopper. The test tube/thermocouple assembly was then inserted into a hollow graphite cylinder resting inside of a furnace. A reference thermocouple was inserted into a vertical hole in the graphite with its tip at the same height as the sample thermocouple. Heating and cooling was performed with the furnace programmed at constant cooling and heating rates of 0.5 K/min and 5 K/min. Data were acquired with a commercial thermocouple logging software.

The thermocouples were calibrated using the melting of pure Sn. Data are reported in DTA type format; i.e., the difference between the sample temperature and the reference temperature is plotted versus the sample temperature. To obtain a flat base line, a test was performed at each heating/cooling rate with an empty sample test tube. The DTA signal from this dummy test was subtracted from that obtained with the alloy samples. In standard DTA or DSC, the sample thermocouple is located just below the sample container. In the present experiments the thermocouple probe is extremely thin, is in direct contact with the alloy and is thus more sensitive than standard methods. Fig. 2 shows the melting and freezing signal for pure Sn at two heating/cooling rates. In contrast to the standard DTA/DSC, the drop of the DTA signal during melting at 231.8 °C is vertical and is not sensitive to heating rate. During cooling (Sn) nucleation occurs approx. 30 °C below the melting point. The recalescence from this temperature is indicated by the positive slope of the DTA signal. The maximum temperature reached is the Sn melting point at 232.0 °C along the short vertical segment. Thus the cooling and heating difference is 0.2 °C.

Standard metallographic examination was performed on selected alloys after cooling at the two rates. Phase identity was confirmed by energy dispersive x-ray analysis in the SEM using elemental standards.

* An error was made in the conversion from atomic to weight % conversion by Miller et al. The composition obtained from the initial estimate was Sn - 3.25 wt % Ag - 0.69 wt % Cu.

* Trade names are used in this paper for completeness only and their use does not constitute an endorsement by NIST.

Results and Discussion

Thermal Analysis

The general solidification behavior of alloys in a simple ternary eutectic system is well known. Solidification consists of three stages (primary, secondary and tertiary) and involves a liquid and three solid phases. If the three solid phases are denoted α, β and γ, the primary stage would be $L \rightarrow \alpha$, the secondary would be $L \rightarrow \alpha+\beta$, and the tertiary would be $L \rightarrow \alpha+\beta+\gamma$. Depending on the alloy composition, the identity of the three phases is permuted. The first two stages occur over a range of temperatures and the third occurs at a fixed temperature. We will call the reaction $L \rightarrow \alpha+\beta$ a monovariant binary eutectic reaction. It is *monovariant* because it has one degree of freedom and *binary* in the sense that only two solid phases form from the liquid. Assuming no nucleation or growth difficulties the following should be possible. During cooling, thermal analysis should be able to detect three temperatures corresponding to the beginning of each stage; i.e., at temperatures at which each new solid phase appears. During heating, thermal analysis should be able to detect three temperatures at which each solid phase finally disappears. In the above example, a signal should be present when all of the γ phase is finally gone, a temperature where all of the β phase is gone, and finally a temperature where all of the α phase is gone. Temperatures obtained on heating and cooling should bracket the true thermodynamic temperature.

The preferred method of thermal analysis is heating. Imperfections in solid structures generally provide ample nucleation sites for phase changes (grain and interphase boundaries). On cooling of a liquid, however, liquid supercooling is often observed. One of the peculiarities of these alloys is the difficulty of observing the liquidus temperature during melting. Thus, data is presented from both heating and cooling. Signals obtained on cooling remain significant because they establish a lower bound on the possible reaction temperature.

Section A – Fig. 3 shows DTA curves for both heating (lower curve) and cooling (upper curve) for alloys from a portion of Section A; viz., from 1.5 wt % Ag-2.7 wt % Cu to 5.0 wt % Ag-1.4 wt % Cu. For brevity, these alloys will be specified by their Ag content only. On heating, the onset of melting is found near 217 °C (see Table 1 for a summary of all results for Section A). The invariant melting process at the ternary eutectic temperature causes a vertical drop in the DTA curve. For the first two alloys in this series (1.5 wt % Ag and 2.5 wt % Ag), a second peak is observed on heating slightly above the ternary eutectic temperature that corresponds to the cessation of one of the monovariant binary eutectic reactions. Upon heating to 300 ºC, it is difficult to distinguish any other signal above the noise. For the other four alloys, only the peak for ternary eutectic melting near 217 ºC is detected.

On cooling, a small peak is seen in each scan well above the ternary eutectic temperature. We will establish that the onset of this peak corresponds to the beginning of primary intermetallic solidification (in this case Cu_6Sn_5). The signal is small because of the very small amount of the phase that was expected in these alloys. The onset of these small peaks are listed in Table 1 as T_L(Cooling). Note in Table 1 that the onset temperatures of these small peaks at the highest temperatures in the scans follow a decreasing trend as the Ag content increases along Section A until 5.0 wt % Ag. Thereafter, it increases as the Ag content increases along Section A as would be expected for the liquidus temperature in a section cutting across the $L \rightarrow Cu_6Sn_5 + Ag_3Sn$ monovariant binary eutectic line.

The DTA scans in Fig. 3 show that during further cooling three of the alloys (4.1, 4.7 and 5.0 wt % Ag) exhibit a second small peak whose onset temperature corresponds to the beginning of the secondary stage of solidification; viz., the monovariant binary eutectic. We will establish that the eutectic is $L \rightarrow Ag_3Sn + Cu_6Sn_5$. The size of these peaks are also small because only a small amount of solid forms by this eutectic. These onset temperatures are recorded in Table 1 as T_B(Cooling); i.e., the monovariant binary eutectic onset temperature during cooling.

Further cooling leads to supercoolings of the order of 20 °C below the ternary eutectic temperature. This is due the difficulty of (Sn) nucleation in these alloys. After nucleation of the (Sn) phase, the maximum temperature reached after recalescence is noted. For the two alloys (1.5 and 2.5 wt % Ag) that had a second peak, this temperature is above the ternary eutectic temperature. It is recorded in Table 1 as T_B(Cooling). Also seen in these two cases is a short vertical segment near the ternary eutectic temperature. For the other alloys (4.1, 4.7, and 5.0 wt % Ag) the maximum recalescence temperature is the ternary eutectic temperature. This is because a monovariant binary eutectic has formed earlier in these three alloys. One also notes the absence of T_B signals for several alloys. Estimated uncertainty (2σ) based on interpretation of the DTA signals is 0.2 K.

Table 1 – Summary of thermal analysis data for section A

Sn wt %	Cu wt %	Ag wt %	Heating			Cooling		
			T_L	T_B	T_E	T_L	T_B	T_E
91.10	0.00	8.90	*295.0*	*221.0*				
91.70	0.30	8.00	287*	220.2	217.6	280.1	219.6	217.1
92.20	0.60	7.20	271*	218.9	217.3	258.2	217.7	217.0
92.50	0.80	6.70	267*	217.9	217.3	262.9	217.9	217.1
92.70	0.90	6.40	264*	217.6	217.3	262.9	213.9^{+}	217.1
92.95	1.05	6.00	n.d.	n.d.	217.2	253.9	223.9	216.9
93.40	1.30	5.30	245*	n.d.	217.2	243.2	237.7	217.0
93.60	1.40	5.00	245*	240.0	217.2	241.7	238.2	216.9
93.80	1.50	4.70	n.d.	236.2	217.2	251.7	233.9	217.1
94.15	1.75	4.10	271*	n.d.	217.2	269.8	224.3	217.1
94.50	2.00	3.50	n.d.	217.9	217.3	278.9	n.d.	217.1
95.20	2.30	2.50	293*	219.8	217.2	290.5	218.9	217.0
95.80	2.70	1.50	309*	222.6	217.3	307.3	221.6	217.0
96.73	3.27	0.00	*325.0*	*227.0*				

Italics – not measured, from binaries
n.d. – not detected
* – measured with cycling experiments
$^{+}$ – large supercooling of (Sn)

Table 2 – Summary of thermal measurements for section B

Sn wt %	Cu wt %	Ag wt %	Heating			Cooling		
			T_L	T_B	T_E	T_L	T_B	T_E
89.51	0.00	10.49	*305.0*	*221.0*				
91.70	0.30	8.00	287*	220.2	217.6	280.1	219.6	217.1
93.40	0.60	6.00	258*	219.2	217.2	257.0	217.9	217.1
94.28	0.72	5.00	244*	218.5	217.3	240.2	n.d.	217.1
94.98	0.82	4.20	226*	218.2	217.4	224.9	n.d.	217.1
95.51	0.90	3.59	n.d.	217.6	217.3	213.6^{+}	217.5	217.0
95.85	0.95	3.20	n.d.	217.8	217.3	203.3^{+}	217.7	217.1
95.96	0.97	3.07	219*	217.8	217.3	220.3	217.9	217.0
96.64	1.07	2.29	232*	221.3	217.4	228.6	218.8	217.0
97.32	1.18	1.50	248*	223.0	217.2	235.3	221.9	216.9
98.64	1.36	0.00	*255.0*	*227.0*				

Italics – not measured, from binaries
n.d. – not detected
* – measured with cycling experiments
$^{+}$ – metastable Ag_3Sn liquidus

Cycling Experiments - Also found in Table 1 are the T_L values for heating for three of the alloys. These data were obtained by thermal cycling experiment following the method described by Wu and Perepezko [8]. In such experiments, a sample was heated to a temperature slightly above the T_L(Cooling) value, held for 3 hours and cooled. If no signal occurrs on cooling, then it is evident that the hold temperature is below the true liquidus; i.e., some solid phase present. This process is repeated at increasing hold temperatures until a signal does occur. By this procedure, the true liquidus could be determined. An example of a cycling experiment is shown in Fig. 4. For the 7.2 wt % Ag alloy in Section A, the true liquidus was 13 K higher than the peak onset observed during cooling. For the other alloys subjected to cycling experiments, T_L(Cooling) and T_L(Heating) are much closer. Cycling experiments were not performed on the other alloys.

The various temperatures are plotted in Fig. 5 for the Section A isopleth. The topology of this diagram was guided by known topology of isopleths through ternary eutectic systems. The absence of T_B signals on heating between 3.5 wt % Ag and 6.4 wt % Ag is now evident. These signals involve the melting of monovariant binary eutectic $Cu_6Sn_5 + Ag_3Sn \rightarrow L$ whose amount is very small.

In Fig. 5, the corners of the three-phase field of $L+Cu_6Sn_5+Ag_3Sn$ at 217.2 °C (6.45 wt % Ag, 0.88 wt % Cu and 3.43 wt % Ag, 1.99 wt % Cu) are very important. These were located precisely using curve fitting of the (L+ Ag_3Sn)/ (L+ (Sn)+ Ag_3Sn) and (L+ Cu_6Sn_5)/ (L+ (Sn)+ Cu_6Sn_5) boundary data obtained on heating. Lines drawn on the ternary composition plot from each of the two intermetallic compositions through these points respectively will intersect at the ternary eutectic composition. Using this construction, we obtain 3.5 wt % Ag and 0.9 wt % Cu. This concentration agrees with that of Loomans and Fine [7] and lies exactly on Section B.

Section B - Table 2 and Fig. 6 summarize the results for Section B. The results are clear except for some uncertainty around 3.5 wt % Ag. Extrapolation of the liquidus curves for the Ag_3Sn and Cu_6Sn_5 phases would intersect below 217 ºC.* This low intersection temperature suggests that Section B cuts through a small piece of the (Sn) phase liquidus surface and that the ternary eutectic composition is slightly to the Cu- and/or Ag-rich side of the section. However, because most of these temperatures were determined on cooling, the two intermetallic liquidus curves could be higher in temperature thereby reducing the concentration range of the (Sn) liquidus in Section B. In fact, the results from Section A concluded that the ternary eutectic composition lies on Section B and would imply that no (Sn) liquidus should appear in Section B. We, therefore, conclude that the ternary eutectic composition may lie at most (0.2 wt %) to the Cu- and/or Ag-rich side of 3.5 wt % Ag, 0.9 wt % Cu.

Metallography

Energy dispersive microprobe x-ray composition analysis was performed on large intermetallics of the Cu_6Sn_5 and Ag_3Sn and a (Sn) dendrite arm to determine the composition of the various phases in as cast samples. The results are shown in Table 3. It can be noted that the Ag solubility in Cu_6Sn_5 and the Cu solubility in Ag_3Sn are quite small. Likewise for the Cu and Ag solubility in (Sn). Because solidification and melting in this system involves phases with negligible solubility ranges, there is little possibility for microsegregation within a phase. Thus predictions of equilibrium (lever) phase diagram calculations are quite valid during melting and solidification. This greatly simplifies the interpretation of DTA signals.

Fig. 7 and Fig. 8 show the microstructure of six of the alloys, labeled A1, A2, A3 in Fig. 5 (Section A) and B1, B2, and B3 in Fig. 6 (Section B). All contain widely separated large intermetallic needles. For alloys A1 and B1, the intermetallic is Ag_3Sn. In A3 and B3, the large intermetallic is Cu_6Sn_5. These observations are consistent with the liquidus curves for the intermetallics identified in Figs. 5 and 6. In alloys A2 and B2, both types of large intermetallics are present. These alloys lie near the $L \rightarrow Cu_6Sn_5 + Ag_3Sn$ monovariant binary eutectic line and the two intermetallics are expected. They grow independently because eutectic reactions between two facetted intermetallic phases do not exhibit coupled growth; i.e., an interposed mixture of the two phases.

The microstructure between the needles compromises approx. 98% of the sample volume and is composed of a dendritic pattern of the (Sn) phase. The dendritic pattern occurs because of the supercooling prior to the formation of (Sn). This supercooling occurs even though large intermetallic particles are present and indicates that the intermetallics are ineffective as heterogeneous nucleation substrates for (Sn). Prior to (Sn) nucleation, but during intermetallic growth, the

* Signals for T_L (Cooling) were obtained below 217 ºC for 3.2 wt % Ag and 3.95 wt % Ag. These temperatures lie on the extrapolated Ag_3Sn liquidus and indicate metastable solidification of Ag_3Sn in the absence of (Sn) and Cu_6Sn_5

Table 3 – Summary of Microprobe Measurements on Phases

	Ag_3Sn			Sn			Cu_6Sn_5		
	Sn	Ag	Cu	Sn	Ag	Cu	Sn	Ag	Cu
Avg. (wt %)	26.88	72.75	0.36	99.74	0.10	0.16	61.66	0.42	37.92
Std. Dev. (wt %)	0.28	0.40	0.12	0.50	0.05	0.07	0.38	0.13	0.31

remaining liquid composition follows the liquidus surface of the intermetallic to lower temperatures and in a composition direction directly away from the composition of the intermetallic. For alloys A2 and B2, the liquid composition follows the line of two-fold saturation between Cu_6Sn_5 and Ag_3Sn.

If (Sn) does not nucleate, either one of these processes causes the remaining liquid composition and temperature to move below the (Sn) liquidus on the metastable extension of the intermetallic liquidus (or metastable extension of the monovariant binary eutectic line). Due the supercooling and the consequently rapid dendritic growth of (Sn), one may also consider that the microstructure between the large intermetallic particles is practically an independent solidification process, having the microstructure of an alloy with composition much more Sn-rich than the original alloy. Analysis of the amount of supercooling and the slopes of the intermediate liquidus surface allows one to estimate the liquid composition at the instant of the start of dendritic growth of (Sn). Between the (Sn) dendrites, Figs. 7 and 8 show various eutectic microstructures. In all alloys except A3 and B3, the sequence of solidification in the region between the large intermetallic consists of dendritic (Sn), monovariant $L \rightarrow (Sn)+Ag_3Sn$, followed by $L \rightarrow (Sn) + Ag_3Sn + Cu_6Sn_5$. In alloy A3 and B3, the sequence is dendritic (Sn), monovariant $L \rightarrow (Sn) + Cu_6Sn_5$, followed by $L \rightarrow (Sn) + Ag_3Sn + Cu_6Sn_5$. Each sequence agrees with that predicted for solidification of the more Sn-rich composition existing at the time of nucleation.

The metallographic sections do not reveal these solidification paths in a straightforward manner. The Ag_3Sn phase is always recognized as elongated plates, usually seen edge-on. The Cu_6Sn phase appears as more blocky particles. Because the two monovariant binary eutectics consist of a facetted and a non-facetted phase (e.g., unlike Sn-Pb), the intermetallics do not always grow in perfect coordination with the (Sn). Thus, the corresponding microstructural regions are not always apparent. The best microstructural feature to separate the stages of solidification is the size of the intermetallic particles. In A1, A2, B1, and B2, the presence of an intermediate size of Ag_3Sn is apparent in addition to very fine Ag_3Sn present during latter (ternary eutectic solidification). In alloys A3 and B3 the intermediate size Ag_3Sn replaced by an intermediate scale of Cu_6Sn_5. This observation leads to our conclusion about the solidification path of the supercooled liquid between the large scale intermetallics. The ternary eutectic microstructure of (Sn) + Ag_3 Sn + Cu_6Sn_5 is shown in Fig. 9a; however, it is not always present. The organization of the growth of this structure may be difficult as it appears to compete with the pair of binary eutectic reactions with the same fine spacings in some regions as shown in Fig.9b. It should be noted that microstructures obtained in solder joints may differ from those presented here.

Phase Diagram Modeling

For multicomponent systems, a preliminary phase diagram can be obtained from extrapolation of the thermodynamic functions of the constituent binary systems. Several methods exist to determine the weighting terms used in such an extrapolation formula. For the present work the extrapolation formula of Muggianu et al. [9] was employed. This preliminary diagram can be used to identify composition and temperature regimes where maximum information can be obtained with minimum experimental effort. With further experimentation, ternary data can then be used to introduce ternary excess parameters into the thermodynamic functions. This procedure was used in the current research. The TERFKT[18], TERGSS[18] and Thermo-Calc software packages were used to carry out the calculations.

The description of the Gibbs energy of a disordered solution phase such as liquid consists of four parts: $G = G^0 + G^{id} + G^{ex}_{bin} + G^{ex}_{ter}$. The term G^0 is prescribed by the description of the constituent elements, G^{id} is the configurational entropy, G^{ex}_{bin} is the sum of the excess terms from the description of the binary systems and G^{ex}_{ter} is the ternary excess term. This term can be symmetric with respect to the concentration of the elements, i.e. $x_1x_2x_3L$, or

asymmetric, $x_1x_2x_3(x_1L_1+x_2L_2+x_3L_3)$. Both cases become identical if $L_1=L_2=L_3$ since $x_1+x_2+x_3=1$. The L parameters can be constant or temperature dependent. The optimization process revealed that there was little difference whether the symmetric function or a form of the asymmetric function, $x_{Ag}x_{Cu}x_{Sn}(x_{Sn}L_{Sn})$, was used. This is not surprising, since the optimization was only concerned with the Sn-rich portion of the system and the contribution of $x_{Ag}L_{Ag}$ and $x_{Cu}L_{Cu}$ to the ternary excess term is fairly small. Therefore, the function $x_{Ag}x_{Cu}x_{Sn}(x_{Sn}L_{Sn})$ was used for the final description as given in the Appendix.

The first calculation of the ternary system was an extrapolation based on the assessments of Ag-Sn from Kattner and Boettinger [10], Cu-Sn from Boettinger et al. [11] and Ag-Cu from Hayes et al. [12]. This gave a ternary eutectic in the Sn-rich corner at 217.4 °C and Sn-3.25 wt % Ag-0.69 wt % Cu. The temperature dependence of the Gibbs energies of the pure elements, the so-called lattice stabilities, used in the above Ag-Sn and Cu-Sn descriptions considered only enthalpy and entropy of transformation. However, for the calculation of thermodynamic properties, such as enthalpy as a function of temperature, it is desirable to include the full temperature dependence of enthalpy and entropy as in SGTE lattice stabilities [13]. These lattice stabilities have become a de facto standard for the description of the pure elements thus providing consistency among descriptions from different assessments. Oh et al. [14] and Shim et al. [15] developed descriptions of the Ag-Sn and Cu-Sn systems, respectively, based on these lattice stabilities. The Cu-Sn assessment of Oh et al. also includes descriptions for all solid phases while the assessment of Boettinger et al. considered only solid phases that exist at temperatures below 350 °C. The description of the Ag-Cu system [17] was readjusted for the use with SGTE lattice stabilities using the experimental data set compiled by Krieg [16]. The extrapolation from these assessments gave a ternary eutectic at 216.9 °C and Sn-3.42 wt % Ag-0.67 wt % Cu.

Attempts to adjust the symmetric ternary parameter, L, of the description of the liquid phase to reproduce the eutectic reported by Miller et al. [5] were not successful. The calculated temperature for the eutectic became unreasonably low when the attempt was made to reproduce this eutectic composition. On the other hand a first approximation could easily be obtained for the eutectic composition reported by Loomans and Fine [7]. This approximation (L = -30 kJ/mol) gave a eutectic at 215.9 °C and Sn-3.74 wt % Ag-0.85 wt % Cu. The diagram obtained from this calculation was used to guide the experimental work described above.

A data set was selected from the present work in which all data from heating and cycling experiments are included and data from cooling experiments when no information from the other experiment was available. These selected data as well as the data from Loomans and Fine [7] and Chada et al. [17] were then used to obtain a refined description of the Gibbs energy of the liquid phase. The program TERGSS by Lukas et al. [18] which uses a least squares method was used for the optimization of the ternary excess parameters. The course of the optimization revealed that it was not possible to obtain a fit within the accuracy of the available experimental data and it became obvious that close attention had to be paid to the accuracy of the fit of the Sn-rich part of the binary systems.

The Cu-Sn Eutectic

Various evaluations of the experimental data of the Cu-Sn binary system agree on the temperature (227 °C) for the Sn-rich eutectic but give two different compositions: 0.9 wt % Cu and 0.7 wt % Cu in the two editions of "Binary Alloy Phase Diagrams" [19]. The slope of the primary (Sn) liquidus is well established, while the data for the Cu_6Sn_5 liquidus scatter significantly. The reported temperatures of the eutectic range from 226.9 °C to 227.1 °C. The composition obtained from the slope of the primary (Sn) liquidus at the eutectic temperature (227 °C) is 0.97 wt % Cu. A eutectic composition of 0.7 wt % Cu would be only in accord with a higher eutectic temperature (228 °C) or a steeper (Sn) liquidus. The calculated eutectic from the assessment of Shim et al. is 226.8 °C and 0.89 wt % Cu, which is in good agreement with the experimental data. However, given the sensitivity of the ternary eutectic temperature to the binary description, the stability of the Cu_6Sn_5 phase was modified slightly to raise the eutectic temperature to 227.0 °C (see Appendix). This resulted in a slightly lower Cu concentration of 0.87 wt % for the eutectic liquid since the slope of the (Sn) liquidus was unchanged. The calculated phase diagram as well as the magnified Sn-rich part of the system is shown in Fig. 10.

The Ag-Sn Eutectic

The experimental data on the eutectic in the Ag-Sn system are in excellent agreement. The reported temperatures range from 221 °C to 221.3 °C and the reported composition is unanimously 3.5 wt % Ag.

Table 4 – Difference between the calculated and measured temperatures from Loomans and Fine [7] for the monovariant eutectics

Phase boundary	wt % Cu	wt % Ag	measured temperature (°C)	ΔT (calculated-measured)
L+Ag_3Sn/	0.25	4.0	220.4	-1.11
L+Ag_3Sn + (Sn)	0.55	4.0	219	-0.71
	0.79	3.6	218	-0.87
L + Cu_6Sn_5/	1.2	1.0	224.2	-0.28
L + Cu_6Sn_5 + (Sn)	1.2	2.0	221.4	-0.44
	1.2	3.0	218.7	-0.64

Although the fit of the experimental data of the assessment of Oh et al. [14] is generally excellent, the calculated eutectic temperature of 220.1 °C is noticeably lower than the experimental temperature. The attempt to readjust the stability of the Ag_3Sn phase in the description of Oh et al.[14] in the same fashion as the Cu_6Sn_5 phase in the Cu-Sn system resulted in a noticeably higher liquidus for this phase. The calculated temperature from the assessment of Kattner and Boettinger [10] is with 220.9 °C closer to the experimental temperature. Therefore, the experimental data compiled by Kattner and Boettinger were used to readjust the description for the use with SGTE lattice stabilities. The eutectic calculated from this description occurs at 220.9 °C and 3.53 wt % Ag (Appendix for description). The calculated phase diagram as well as the magnified Sn-rich part of the system is shown in Fig. 11.

The Ag-Cu-Sn Eutectic

The revised descriptions of the Ag-Sn and Cu-Sn systems were used for the optimization of the values of the parameters of the ternary excess term. Despite the effort on improving the descriptions of the binary systems, 216.3 °C and Sn-3.66 wt % Ag-0.91 wt % Cu was the best fit to the eutectic from the above experimental work that could be obtained. The calculated isopleths and the experimental data from the present work are compared in Fig. 12. The data from Chada et al. [17] which were obtained from the isothermal saturation of a Sn-3.5 wt % Ag eutectic solder with Cu are compared with the calculated liquidus in Fig. 13. The results of Loomans and Fine [7] for the monovariant eutectics are compared with the calculated temperatures in Table 4. The calculated Sn-rich liquidus surface and surface of secondary crystallization are shown in Fig. 14 and isothermal sections are shown in Fig. 15. The final description used for these calculations is given in the Appendix.

It can be seen from Figs. 12 and 13 and Table 4 that the calculation of the Sn-rich corner reproduces the experimental data well. However, the result of calculation is not within the accuracy of the experiment whose standard deviation is 0.2 K. It should be noted that the calculated invariant equilibrium L + $Cu_3Sn \rightarrow Ag_3Sn + Cu_6Sn_5$ (352.5 °C, Sn-18.2 wt % Ag-6.4 wt % Cu) also is in good agreement with the experimental data, 350 °C, Sn-20 wt % Ag-6 wt % Cu by Gebhardt and Petzow [3] and 350 °C by Fedorov et al. [4], even though these data were not used for the optimization. For further refinement of the thermodynamic description it is necessary to improve the description of the binary Ag-Sn and Cu-Sn liquid phase and the Ag_3Sn and Cu_6Sn_5 phases. It can be seen from the magnified Sn-rich part of the phase diagram in Figs. 10b and 11b that the experimental data for the liquidus of the intermetallic phase reveal noticeable scatter. Experimental data with an accuracy similar to the accuracy of the ternary data are needed for the improvement of the description of these phases.

Simulation of DTA signals

A simple model for heat flow between the sample and the furnace [20] was developed to predict the sample temperature as a function of time for understanding the difficulty of the liquidus measurement during heating in these alloys. A single thermal response time between the sample and the furnace wall is obtained by fitting the model to the data obtained for pure Sn. This response time is related to the time that it takes the DTA signal to return to the baseline after the end of melting. Using the thermodynamic assessment, the enthalpy versus temperature curve was computed for one of the alloy compositions, Sn -2.5 wt % Ag- 2.3 wt % Cu. It is shown in the top part of Fig. 16. Using this curve and the heat flow model, the DTA curves were computed for 0.5 K/min. heating rates and compared to those obtained experimentally (Figs. 16, bottom). The very

small signal obtained at the liquidus temperature corresponding to the very small change in the slope of the enthalpy vs. temperature curve is evident. This is consistent with the small or undetectable signal in the experiments. The signal associated with the monovariant binary eutectic is accurately reproduced by the simulation.

The reason for the stronger signal on cooling at the liquidus than for melting is not completely clear. It may be due to the small amount of supercooling (generally about 5-10 K prior to the nucleation of the intermetallic phases that makes the initial growth more rapid than would normally occur. Thus a larger amount of heat of fusion is released in a short time.

Summary

1) From thermal analysis during heating and cooling and from metallography, the phase diagram of the Sn-rich corner of the Sn-Ag-Cu system has been established. The location of the ternary eutectic composition is consistent with that obtained by Loomans and Fine [7] and not Miller et al. [5]. The present results indicate the eutectic composition to be 3.5 wt % Ag ± 0.3 wt % Ag and 0.9 wt % Cu ± 0.2 wt % at 217.2 °C ± 0.2 °C. The composition errors are more likely to be in the Cu and/or Ag direction.

2) The calculated phase diagram satisfactorily reproduces the experimental data - but not within the accuracy of the experimental data. The calculation revealed that for an improved description of the ternary system the descriptions of the binary Ag-Sn and Cu-Sn systems need further refinement requiring experimental data with an accuracy similar to the accuracy of the ternary data.

3) The simulation of DTA signals using an enthalpy vs. temperature curve obtained from the thermodynamic calculation indicates the reasons for the difficulty of intermetallic liquidus measurements in these alloys.

Acknowledgement

The authors thank H. L. Lukas for providing the thermodynamic software (TERGSS and TERFKT).

References

1. NCMS Report 0401RE96, *Lead-Free Solder Project*, National Center for Manufacturing Sciences, Ann Arbor, MI, August 1997 (CD-ROM, June 1998).
2. J. Bath, C.A. Handwerker and E. Bradley, *NEMI Group Recommends "Standardized" Lead-Free Solder Alternative*, to be submitted to *Circuit Assembly Magazine.*
3. E. Gebhardt and G. Petzow, *Z. Metallkde.* 50, 597 (1959).
4. V.N. Fedorov, O.E. Osinchev and E.T. Yushkina referenced in *Phase Diagrams of Metallic Systems, Vol. 26*, Eds. N.V. Ageev and L.A. Petrova, VINITI, Moscow, USSR, 1982, pp.149-150.
5. C.M. Miller, I.E. Anderson and J.F. Smith, *J. Electron. Mater.* 23, 595 (1994).
6. U.S. Patent No. 5,527,628 (1996).
7. M.E. Loomans and M.E. Fine, *Metall. Mater. Trans. A* 31A 1155 (2000).
8. R. I. Wu and J. H. Perepezko, *Metall. Mater. Trans. A* 31A, 497 (2000).
9. Y.-M. Muggianu, M. Gambino and J.-P. Bros, *J. Chim. Phys.* 72, 85 (1975).
10. U.R. Kattner and W.J. Boettinger, *J. Electron. Mater.* 23, 603 (1994).
11. W.J. Boettinger, C.A. Handwerker and U.R. Kattner, *Reactive Wetting and Intermetallic Formation*, in *The Mechanics of Solder Alloy Wetting and Spreading*, Eds. F.G. Yost, F.M. Hosking and D.R. Frear, Van Nostrand Reinhold, New York, NY, USA, 1993, pp. 103-140.
12. F.H. Hayes, H.L. Lukas, G. Effenberg and G. Petzow, *Z. Metallkde.* 77, 749 (1986).
13. A.T. Dinsdale, *CALPHAD* 15, 317 (1991).
14. C.-S. Oh, J.-H. Shim, B.-J. Lee and D.N. Lee, *J. Alloys Compds*. 238, 155 (1996).
15. J.-H. Shim, C.-S. Oh, B.-J. Lee and D.N. Lee, *Z. Metallkde*. 87, 205 (1996).
16. H. Krieg, unpublished research, Max-Planck-Institut für Metallforschung, Stuttgart, Germany, 1982.
17. S. Chada, W. Laub, R.A. Fournelle and D. Shangguan, *J. Electron. Mater.* 28, 1194 (1999).
18. H.L. Lukas, E.Th. Henig and B. Zimmermann, *CALPHAD* 1, 225 (1977).
19. T.B. Massalski (Ed. in chief), *Binary Alloy Phase Diagrams*, ASM International, Materials Park, 1st ed., 1986, pp. 964-965, 2nd ed., 1990, pp. 1481-1483.
20. W.J. Boettinger, unpublished research, NIST, Gaithersburg MD, 2000.
21. P.-Y. Chevalier, *Thermochim. Acta* 136, 45 (1988).
22. T.L. Ngai and Y.A. Chang, *CALPHAD* 5, 267 (1981).
23. I.Ansara, LPTCM-ENSEEG, Grenoble, France, private communication, 1993.
24. 24. B.-J. Lee, KRISS, Taejon, South Korea, private communication, 1999.

Appendix: Analytical Description of the Sn-Ag-Cu System

Functions for the Pure Elements

GHSERAG (Dinsdale[13]) =
298.15 K < *T* < 1234.93 K:
-7209.512 +118.202013 *T* -23.8463314 *T* ln *T* -.001790585 T^2 -3.98587 x 10^{-7} T^3 -12011 T^{-1}
1234.93 K < *T* < 3000.00 K:
-15095.252+190.266404 *T* -33.472 *T* ln *T*+1.412 x 10^{29} T^{-9}
GAGLIQ (Dinsdale [13]) =
298.15 K < *T* < 1234.93 K: +11025.076 -8.891021 *T* -1.034 x 10^{-20} T^7 +GHSERAG
1234.93 K < *T* < 3000.00 K: +11508.141 -9.301747 *T* -1.412 x 10^{29} T^{-9}+GHSERAG
GAGHCP (Dinsdale [13]) =
298.15 K < *T* < 3000.00 K: +300.0 +0.30 *T* +GHSERAG
GAGBCT (Chevalier[21]) =
298.15 K < *T* < 3000.00 K: +4184.1 +GHSERAG

GHSERCU (Dinsdale [13]) =
298.15 K < *T* < 1357.77 K: -7770.458 +130.485235 *T* -24.112392 *T* ln *T* -.00265684 T^2 +1.29223 x 10^{-7} T^3 +52478 T^{-1}
1357.77 K < *T* < 3200.00 K: -13542.026 +183.803828 *T* -31.38 *T* ln *T* +3.642 x 10^{29} T^{-9}
GCULIQ (Dinsdale [13]) =
298.15 K < *T* < 1357.77 K: +12964.736 -9.511904 *T* -5.849 x 10^{-21} T^7 +GHSERCU
1357.77 K < *T* < 3200.00 K: +13495.481 -9.922344 *T* -3.642 x 10^{29} T^{-9} +GHSERCU
GCUBCC (Dinsdale [13]) =
298.15 K < *T* < 3200 K: +4017.0-1.255 *T*+GHSERCU
GCUBCT =
298.15 K < *T* < 3200 K: +4184.0+GHSERCU

GHSERSN (Dinsdale [13]) =
250.00 K < *T* < 505.08 K: -5855.135 +65.443315 *T* -15.961 *T* ln *T* -.0188702 T^2 +3.121167 x 10^{-6} T^3 –61960 T^{-1}
505.08 K < *T* < 800.00 K: +2524.724 +4.005269 *T* -8.2590486 *T* ln *T* -.016814429 T^2 +2.623131 x 10^{-6} T^3 -1081244 T^{-1}
-1.2307 x 10^{25} T^{-9}
800.00 K < *T* < 3000.00 K: -8256.959 +138.99688 *T* -28.4512 *T* ln *T* -1.2307 x 10^{25} T^{-9}
GSNLIQ (Dinsdale [13]) =
100.00 K < *T* < 505.08 K: +7103.092 -14.087767 *T* +1.47031 x 10^{-18} T^7 +GHSERSN
505.08 K < *T* < 3000.00 K: +6971.587 -13.814382 *T* +1.2307 x 10^{25} T^{-9} +GHSERSN
GSNFCC (Ngai and Chang[22]) =
298.15 K < *T* < 3000 K: 5510-8.46 *T*+GHSERSN
GSNBCC (Dinsdale [13]) =
298.15 K < *T* < 3000 K: 4400.0-6.00 *T*+GHSERSN
GSNHCP (Ansara[23]) =
298.15 K < *T* < 3000 K: 3900-7.646 *T*+GHSERSN

Solution Phases

Phase Liquid (Constituents Ag, Cu, Sn)
G(Liquid,Ag) - H^{SER}_{Ag} = GLIQAG
G(Liquid,Cu) - H^{SER}_{Cu} = GLIQCU
G(Liquid,Sn) - H^{SER}_{Sn} = GLIQSN
L(Liquid,Ag,Cu;0) = +17323.40-4.46819 *T*
L(Liquid,Ag,Cu;1) = +1654.38-2.35285 *T*
L(Liquid,Ag,Sn;0) = -4908.72-4.70156 *T*
L(Liquid,Ag,Sn;1) = -16987.99+4.93677 *T*
L(Liquid,Ag,Sn;2) = -6840.22
L(Liquid,Cu,Sn;0) = -9002.8-5.8381 *T* (Shim et al.[15])
L(Liquid,Cu,Sn;1) = -20100.4+3.6366 *T* (Shim et al. [15])
L(Liquid,Cu,Sn;2) = -10528.40 (Shim et al. [15])
L(Liquid,Ag,Cu,Sn;2) = 10416.06-107.98375 *T*

Phase fcc_A1 (Constituents Ag, Cu, Sn)

G(fcc_A1,Ag) - H^{SER}_{Ag} = GHSERAG
G(fcc_A1,Cu) - H^{SER}_{Cu} = GHSERCU
G(fcc_A1,Sn) - H^{SER}_{Sn} = GSNFCC
L(fcc_A1,Ag,Cu;0) = +36061.88-10.44288 *T*
L(fcc_A1,Ag,Cu;1) = -4310.12
L(fcc_A1,Ag,Sn;0) = 4381.80+12.57706 *T*
L(fcc_A1,Ag,Sn;1) = -41594.5
L(fcc_A1,Cu,Sn;0) = -11106.95+2.07910 *T* (Lee[24])
L(fcc_A1,Cu,Sn;1) = -15718.02+5.92547 *T* (Lee[24])

Phase bct_A5 (Constituents Ag, Cu, Sn)
G(bct_A5,Ag) - H^{SER}_{Ag} = GAGBCT
G(bct_A5,Cu) - H^{SER}_{Cu} = GCUBCT
G(bct_A5,Sn) - H^{SER}_{Sn} = GHSERSN
L(bct_A5,Ag,Cu;0) = 20000
L(bct_A5,Ag,Sn;0) = 18706.02
L(bct_A5,Cu,Sn;0) = 21000.0

Semistoichiometric Phases

Phase bcc_A2 (Constituents Cu, Sn)
G(bcc_A2,Cu) - H^{SER}_{Cu} = GCUBCC
G(bcc_A2,Sn) - H^{SER}_{Sn} = GSNBCC
L(bcc_A2,Cu,Sn;0) = -44821.6+51.2164 *T* (Shim et al. [15])
L(bcc_A2,Cu,Sn;1) = -6876.5-56.4271 *T* (Shim et al. [15])

Phase hcp_A3 (Constituents Ag, Sn)
G(hcp_A3,Ag) - H^{SER}_{Ag} = GAGHCP
G(hcp_A3,Sn) - H^{SER}_{Sn} = GSNHCP
L(hcp_A3,Ag,Sn;0) = 297.67+10.62798 *T*
L(hcp_A3,Ag,Sn;1) = -38953.88

Phase DO3 (2 Sublattices 0.75:0.25; Constituents Cu, Sn :Cu ,Sn)
G(DO3,Cu:Cu) - H^{SER}_{Cu} = GCUBCC
G(DO3,Sn:Sn) - H^{SER}_{Sn} = GSNBCC
G(DO3,Cu:Sn) - 0.75 H^{SER}_{Cu} - 0.25 H^{SER}_{Sn} = -10029.85 +0.00285 *T* +0.75 GCUBCC +0.25 GSNBCC (Shim et al. [15])
G(DO3,Sn:Cu) - 0.25 H^{SER}_{Cu} - 0.75 H^{SER}_{Sn} = 116674.85 +4.8166 *T* +0.75 GSNBCC +0.25 GCUBCC (Shim et al. [15])
L(DO3,Cu:Cu,Sn;0) = -1857.8-2.5311 *T* (Shim et al. [15])
L(DO3,Cu:Cu,Sn;1) = -2.9894 *T* (Shim et al. [15])
L(DO3,Cu,Sn:Sn;0) = 45850.0-42.2191 *T* (Shim et al. [15])

Stoichiometric Phases

Phase Ag_3Sn (2 Sublattices 0.75:0.25; Constituents Ag :Sn)
G(Ag_3Sn,Ag:Sn) - 0.75 H^{SER}_{Ag} - 0.25 H^{SER}_{Sn} = -4563.81 -1.40350 *T* +0.75 GAGHCP +0.25 GSNHCP

Phase $Cu_{41}Sn_{11}$ (2 Sublattices 0.788:0.212; Constituents Cu :Sn)
G($Cu_{41}Sn_{11}$,Cu:Sn) - 0.788 H^{SER}_{Cu} - 0.212 H^{SER}_{Sn} = -6323.5 -1.2808 *T* +0.788 GHSERCU +0.212 GHSERSN (Shim et al. [15])

Phase $Cu_{10}Sn_3$ (2 Sublattices 0.769:0.23; Constituents Cu :Sn)
G($Cu_{10}Sn_3$,Cu:Sn) – 0.769 H^{SER}_{Cu} - 0.231 H^{SER}_{Sn} = -6655.0 -1.4483 *T* +0.769 GHSERCU +0.231 GHSERSN (Shim et al. [15])

Phase Cu_3Sn (2 Sublattices 0.75:0.25; Constituents Cu :Sn)
G(Cu_3Sn,Cu:Sn) - 0.75 H^{SER}_{Cu} - 0.25 H^{SER}_{Sn} = -8194.2 -0.2043 *T* +0.75 GHSERCU +0.25 GHSERSN (Shim et al. [15])

Phase Cu_6Sn_5 (2 Sublattices 0.545:0.455; Constituents Cu :Sn)
G(Cu_6Sn_5,Cu:Sn) - 0.545 H^{SER}_{Cu} - 0.455 H^{SER}_{Sn} = -7085.92 +0.15558 *T* +0.545 GHSERCU +0.455 GHSERSN

Phase Cu_6Sn_5_L (2 Sublattices 0.545:0.455; Constituents Cu :Sn)
G(Cu_6Sn_5_L,Cu:Sn) - 0.545 H^{SER}_{Cu} - 0.455 H^{SER}_{Sn} = -7346.12 +0.72038 *T* +0.545 GHSERCU +0.455 GHSERSN

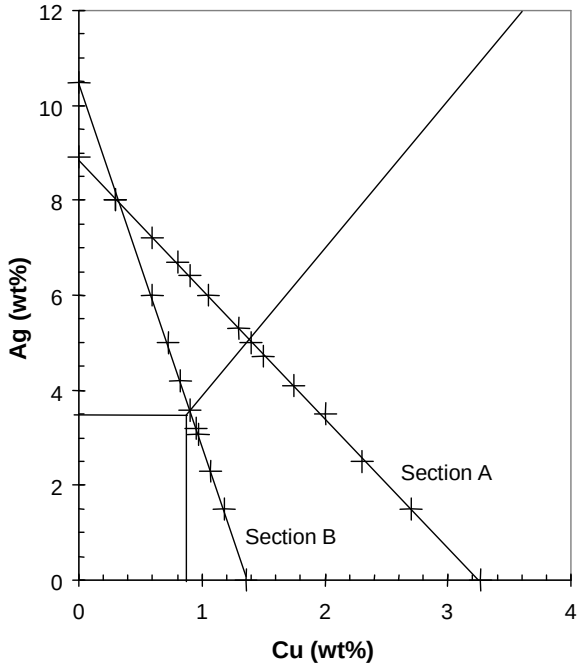

Figure 1. Alloy compositions studied in this research lie along two sections of the Sn-Ag-Cu ternary system. The approximate locations of the three lines of monovariant binary eutectic reaction (lines of two-fold saturation) are shown with an intersection at the ternary eutectic composition determined by Loomans and Fine [7].

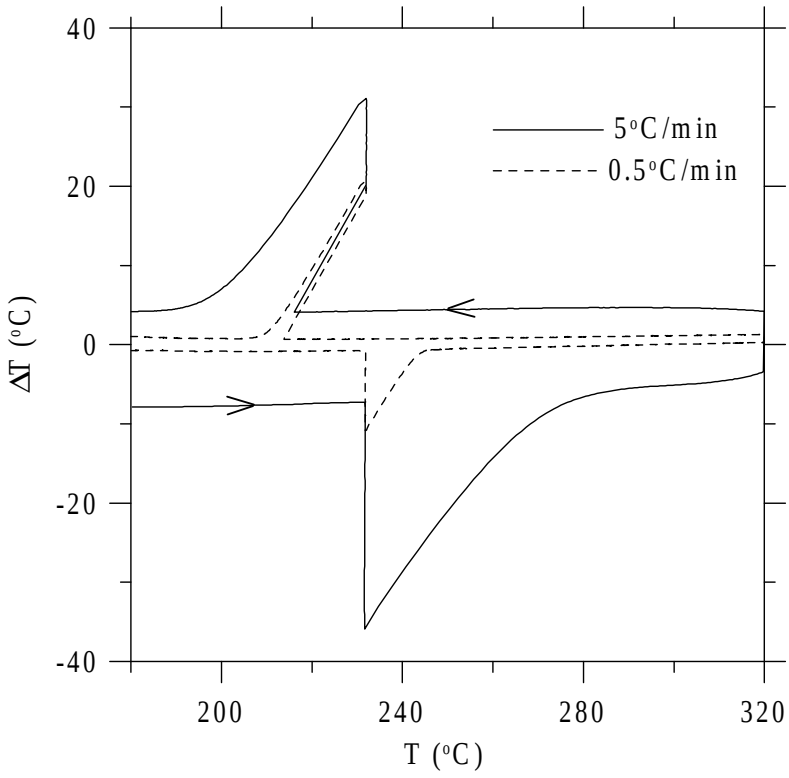

Figure 2. Measured DTA plot for pure Sn at 0.5 K/min and 5 K/min.

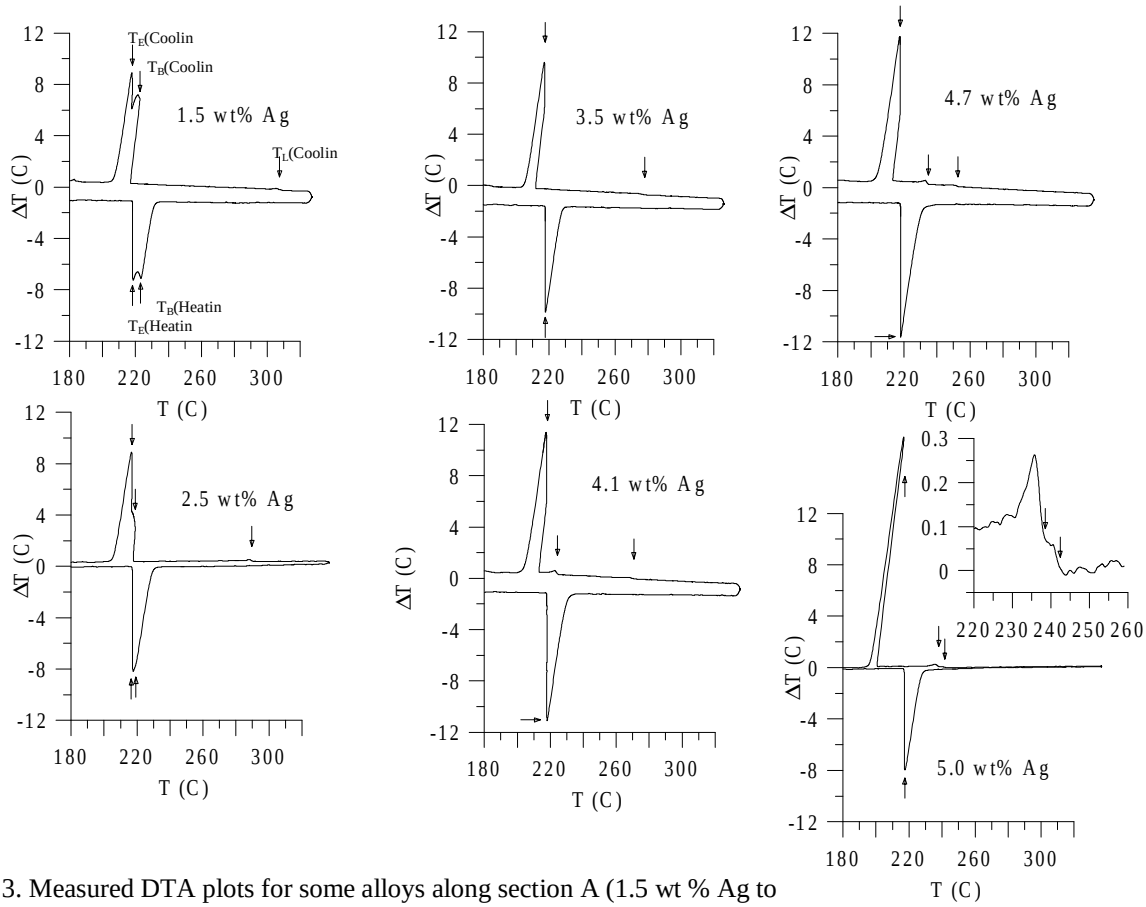

Figure 3. Measured DTA plots for some alloys along section A (1.5 wt % Ag to 5.3 wt % Ag). All of these alloys exhibit primary solidification of Cu_6Sn_5.

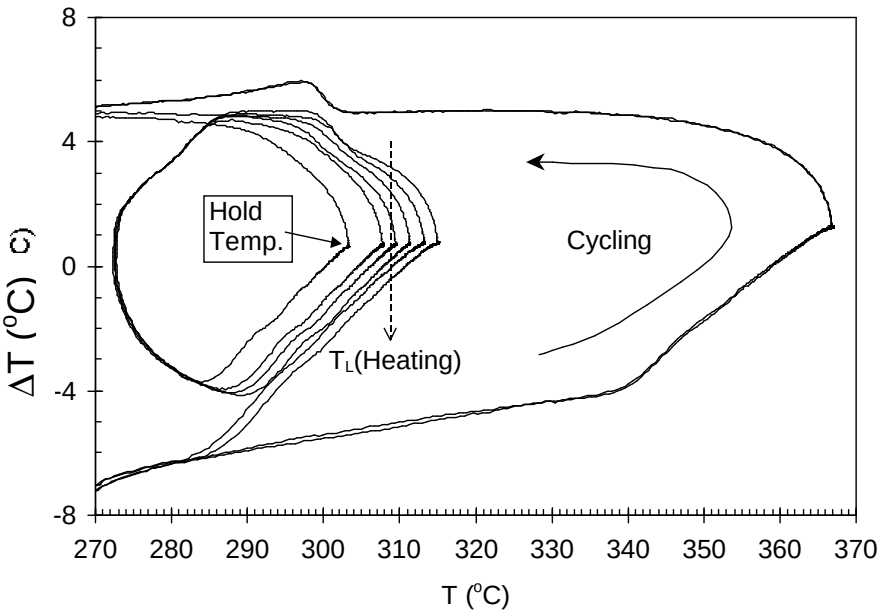

Figure 4. Cycling DTA data for Sn-1.5 wt % Ag-2.7 wt % Cu held at successively higher temperature (left to right: 303.3 ºC, 308.7 ºC, 309.5 ºC, 311.3 ºC, 314.0 ºC, 315.0 ºC, and 366.8 ºC). The heating and cooling rate was 5 ºC/min. The appearance of an inflection point on the startup transient indicates that the liquidus temperature lies between 308.7 ºC and 309.5 ºC

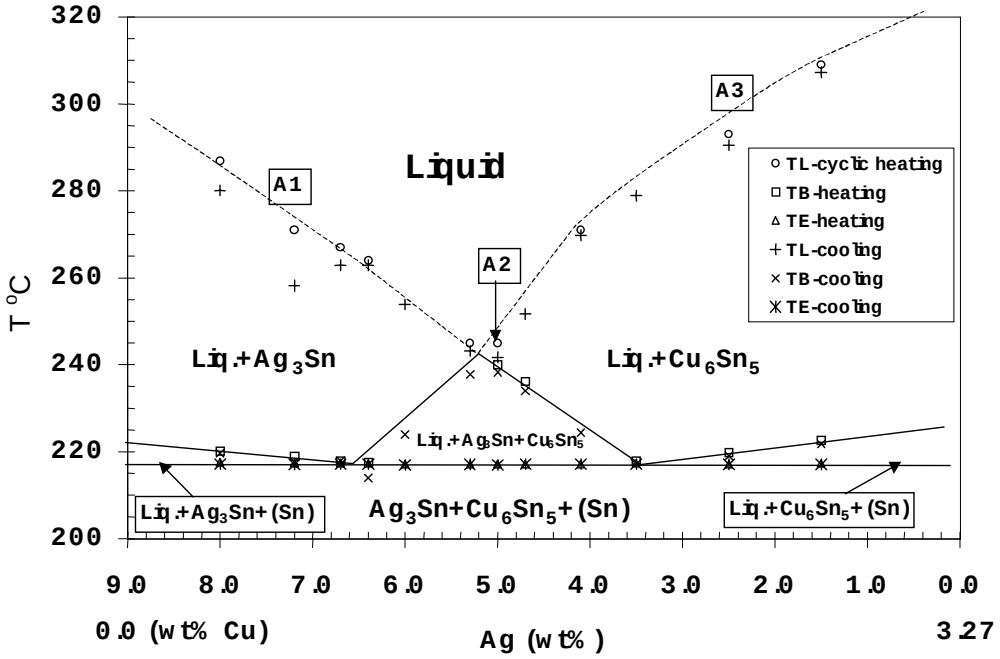

Figure 5. Plot of experimentally determined phase boundaries for Section A.

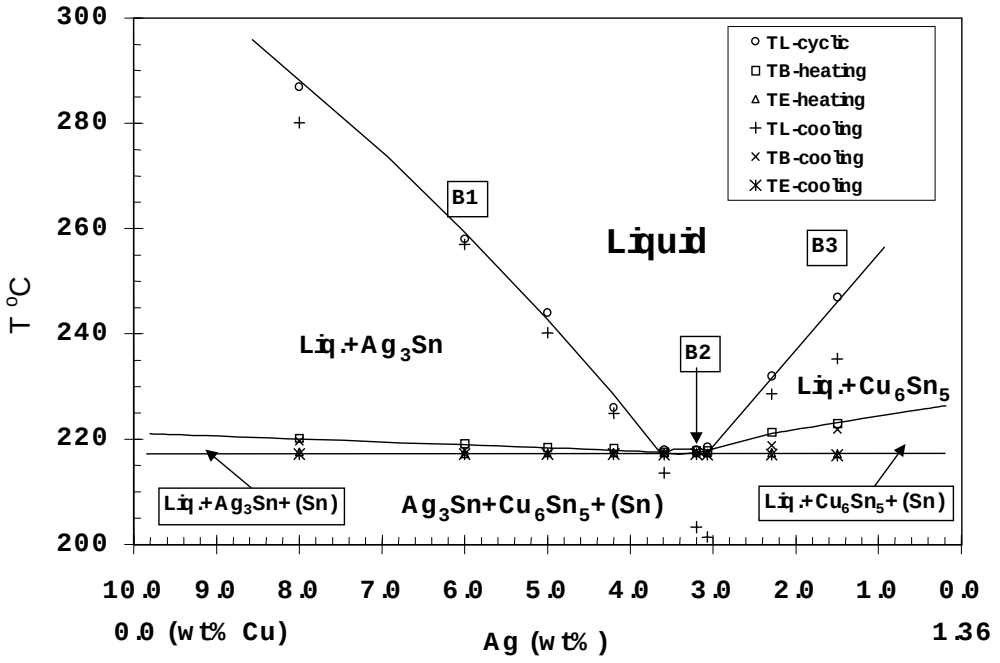

Figure 6. Plot of experimentally determined phase boundaries for Section B.

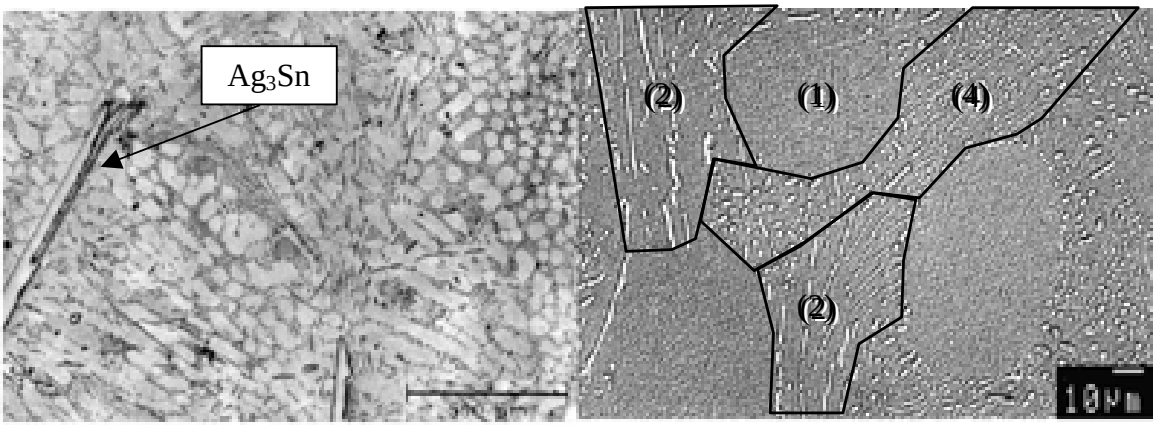

(a) Alloy A1: Sn-7.2wt%Ag-0.6wt%Cu

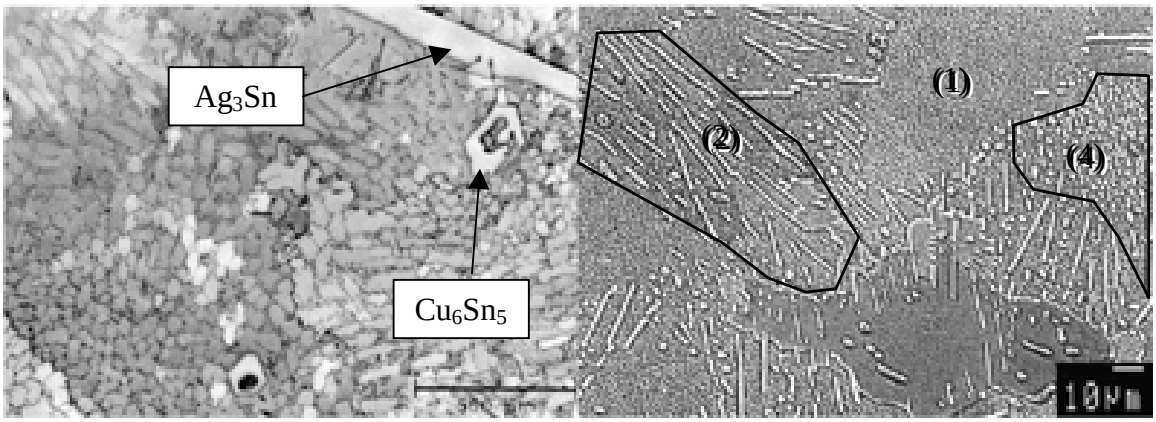

(b) Alloy A2: Sn-5.0wt%Ag-1.4wt%Cu

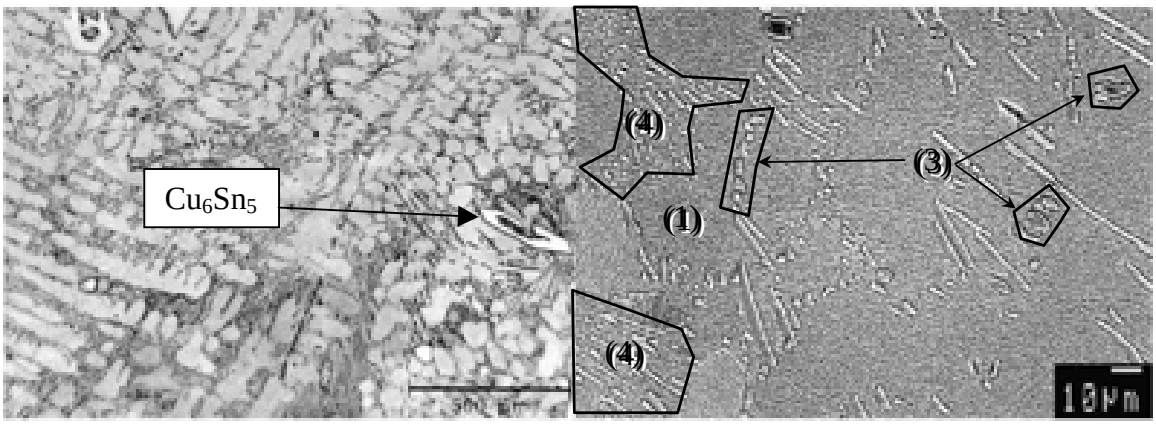

(c) Alloy A3: Sn-2.5wt%Ag-2.3wt%Cu

Figure 7. The left side of optical micrographs of three alloys on section A showing large intermetallic particles and dendritic (Sn) substructure formed from the remaining supercooled liquid. The right side of SEM (backscattered) view indicating examples of various regions: **1** - (Sn); **2** - (Sn) + Ag_3Sn; **3** – (Sn) + Cu_6Sn_5; **4** – (Sn) + Ag_3Sn + Cu_6Sn_5.

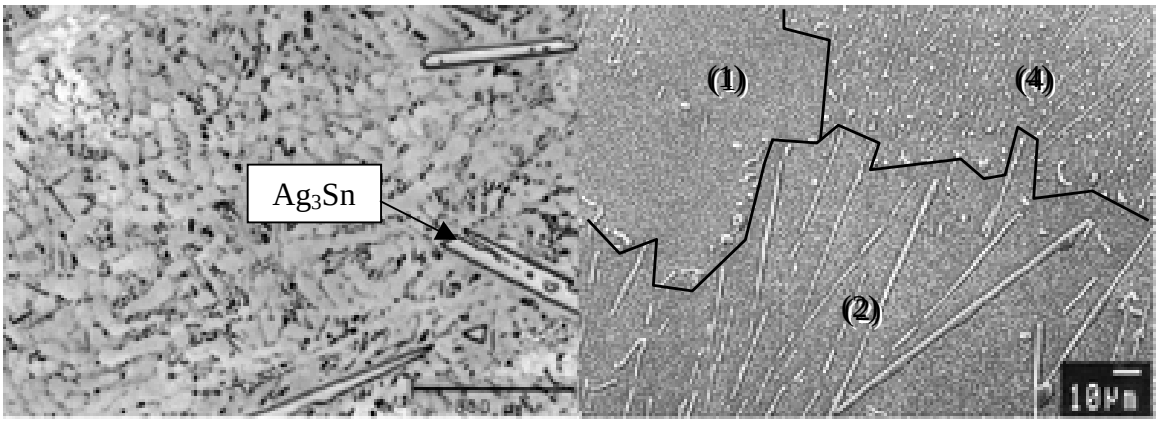

(a) Alloy B1: Sn-6.0wt%Ag-0.6wt%Cu

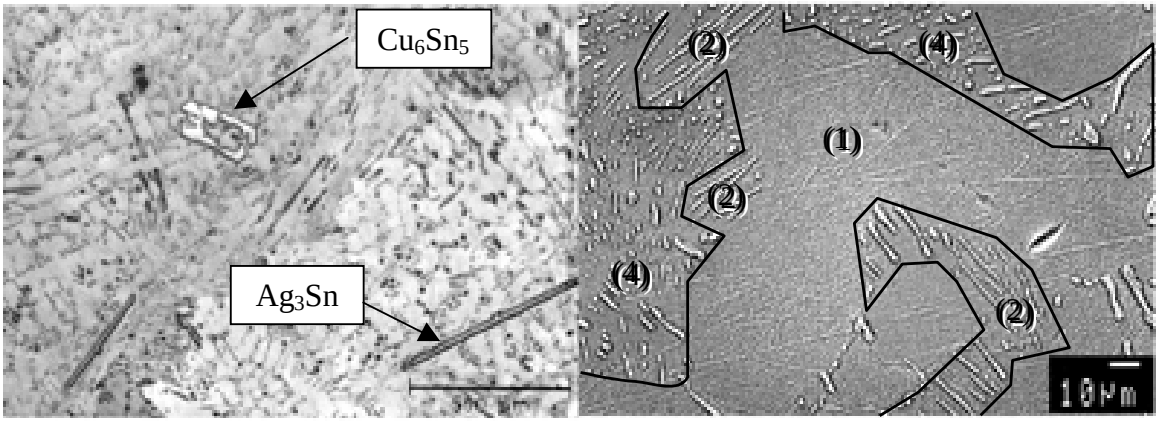

(b) Alloy B2: Sn-3.2wt%Ag-0.95wt%Cu

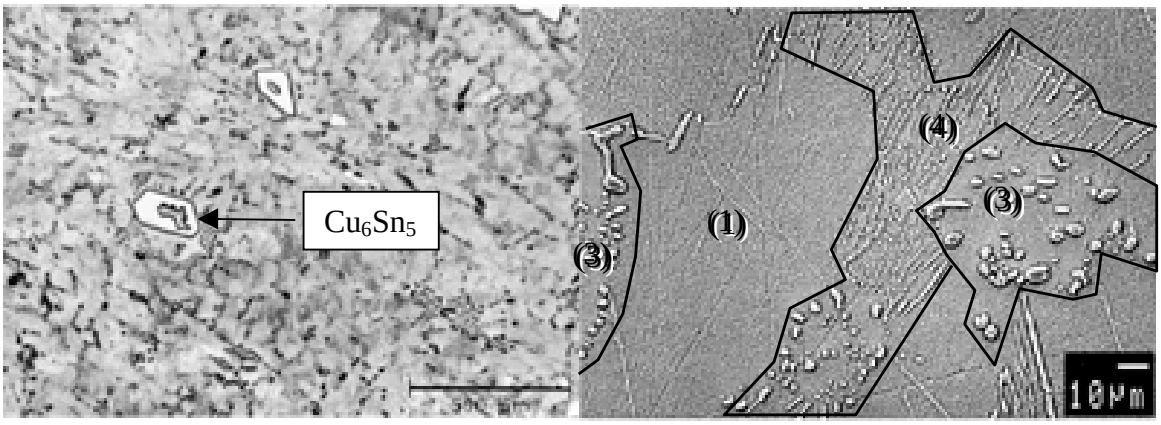

(c) Alloy B3: Sn-1.5wt%Ag-1.18wt%Cu

Figure 8. The left side of optical micrographs of three alloys on section B showing large intermetallic particles and dendritic (Sn) substructure formed from the remaining supercooled liquid. The right side of SEM (backscattered) view. Region labels as in Fig. 7.

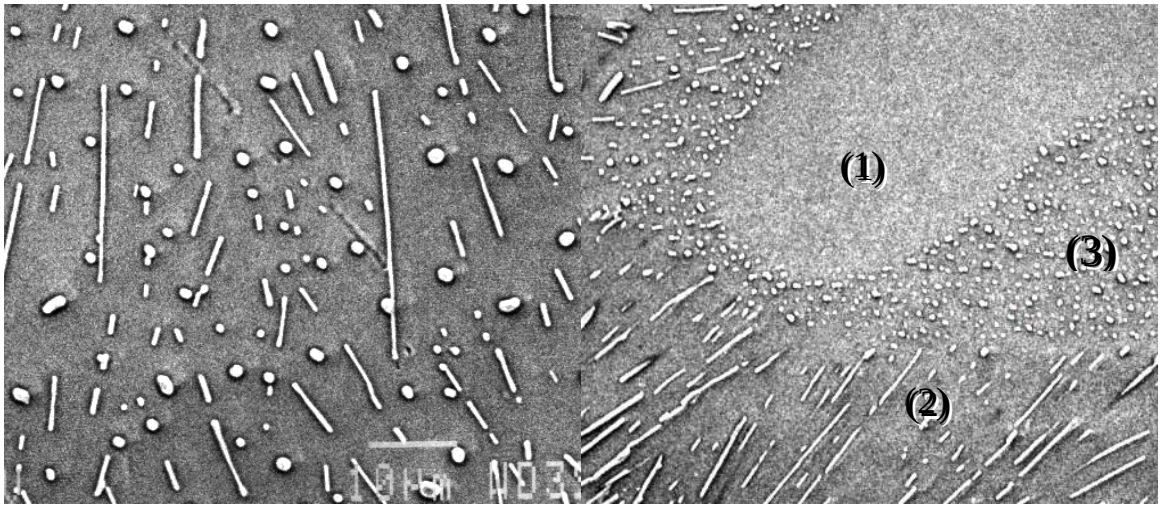

a **b**

Figure 9. SEM micrographs of eutectic structures: (A) ternary eutectic structure (matrix: (Sn), needle shape: Ag_3Sn, and disk shape: Cu_6Sn_5). (B) region with co-existing (Sn)+Cu_6Sn_5 and (Sn)+Ag_3Sn fine two phase regions near a (Sn) dendrite arm. Region labels as in Fig. 7.

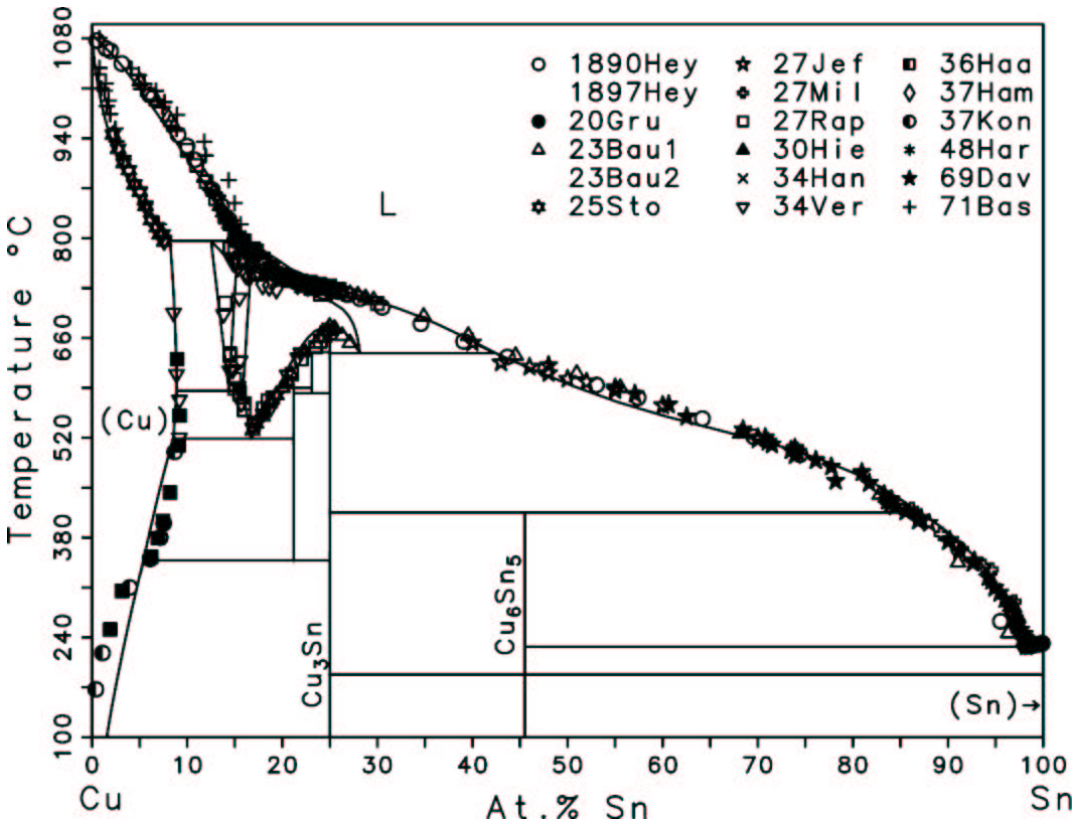

a

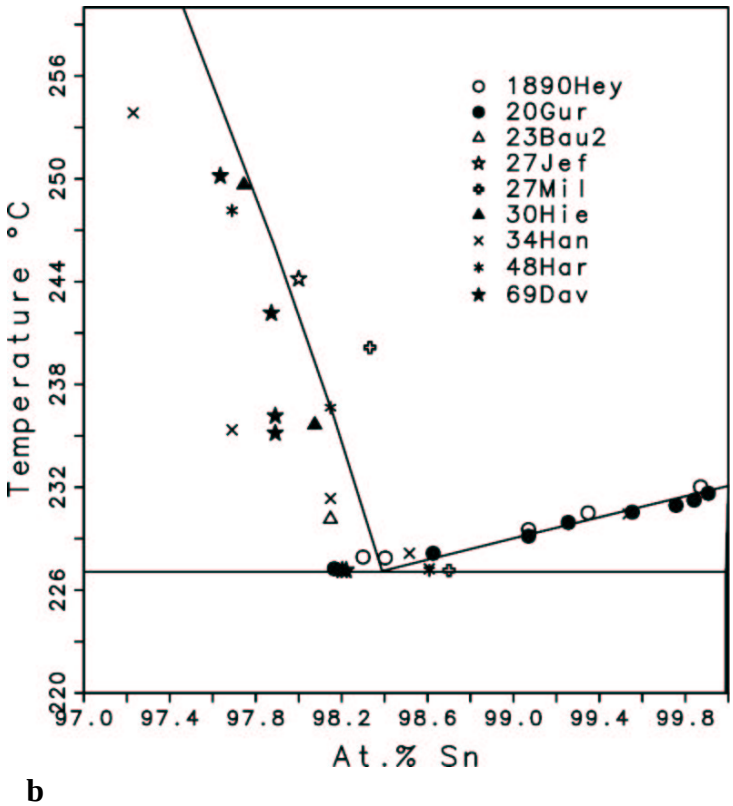

b

Figure 10. Calculated Cu-Sn system. Description from Shim et al. [15], Cu_6Sn_5 description modified in present work. a) phase diagram b) Sn-rich portion. The references for the experimental data shown are given by Boettinger et al. [11].

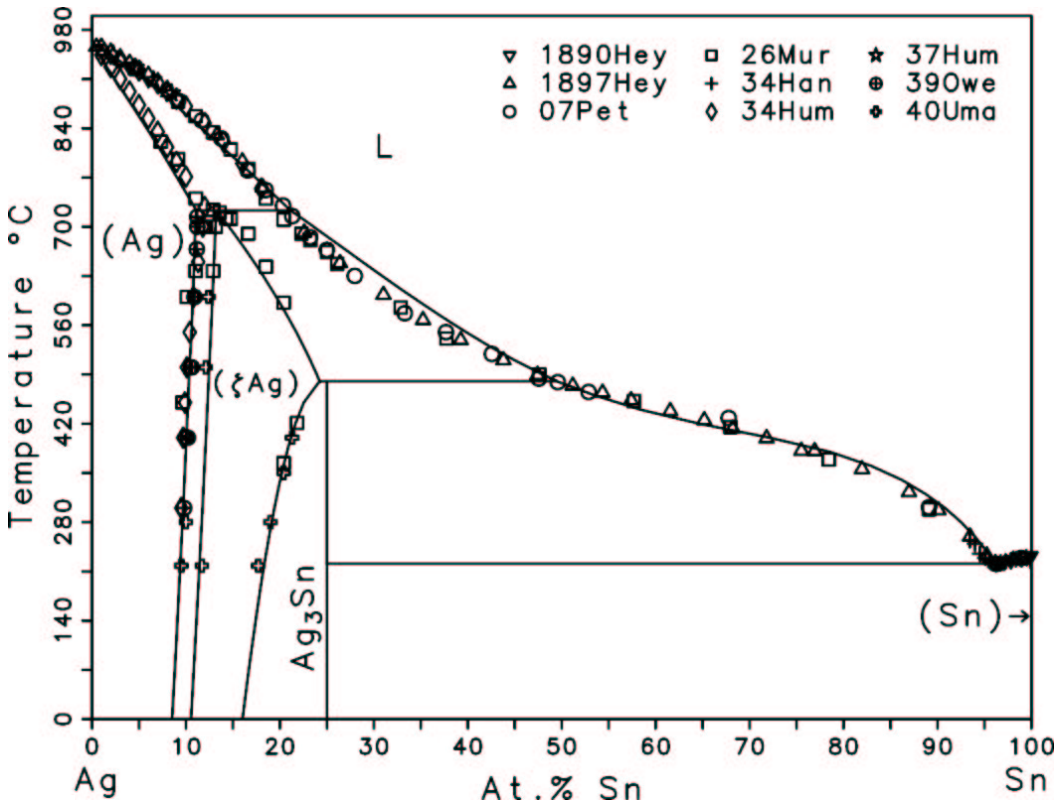

a

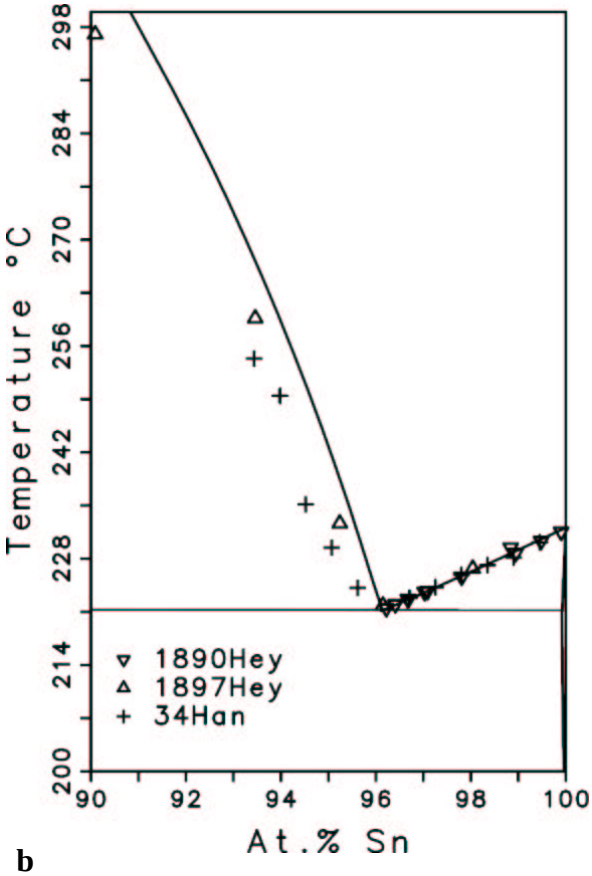

b

Figure 11. Calculated Ag-Sn system. a) phase diagram b) Sn-rich portion. The references for the experimental data shown are given by Kattner and Boettinger [10].

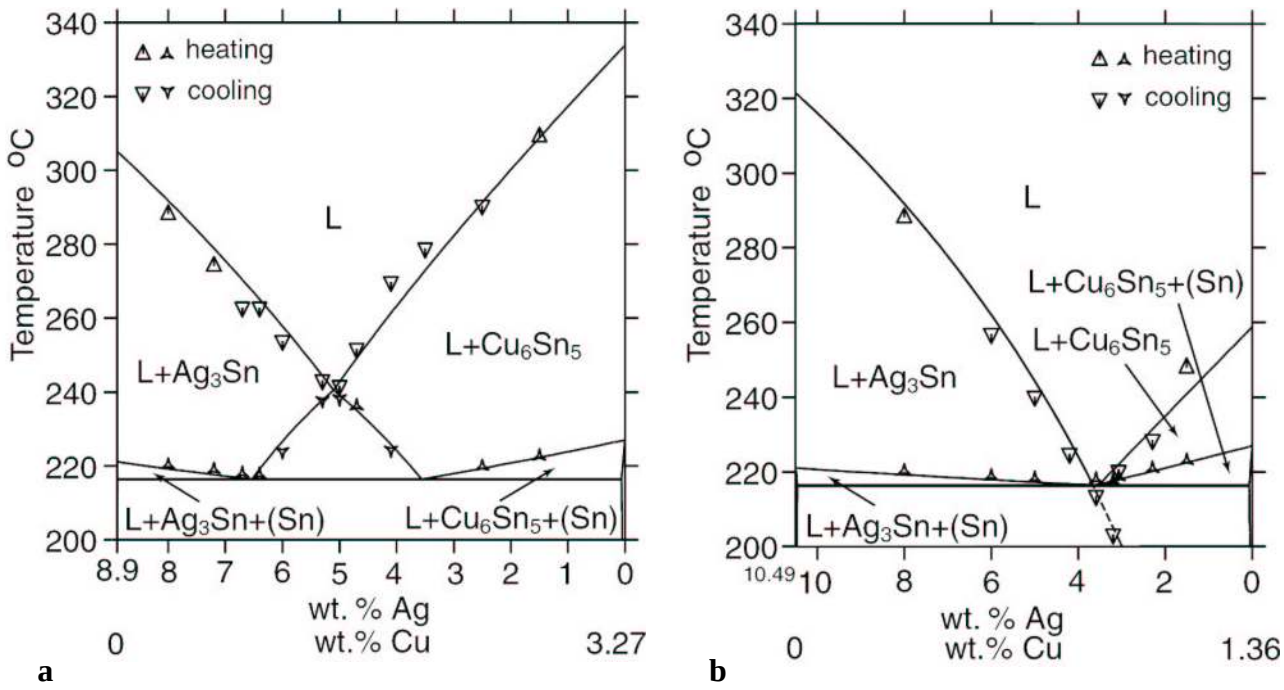

Figure 12. Calculated isopleths and experimental points. a) section A, b) section B.

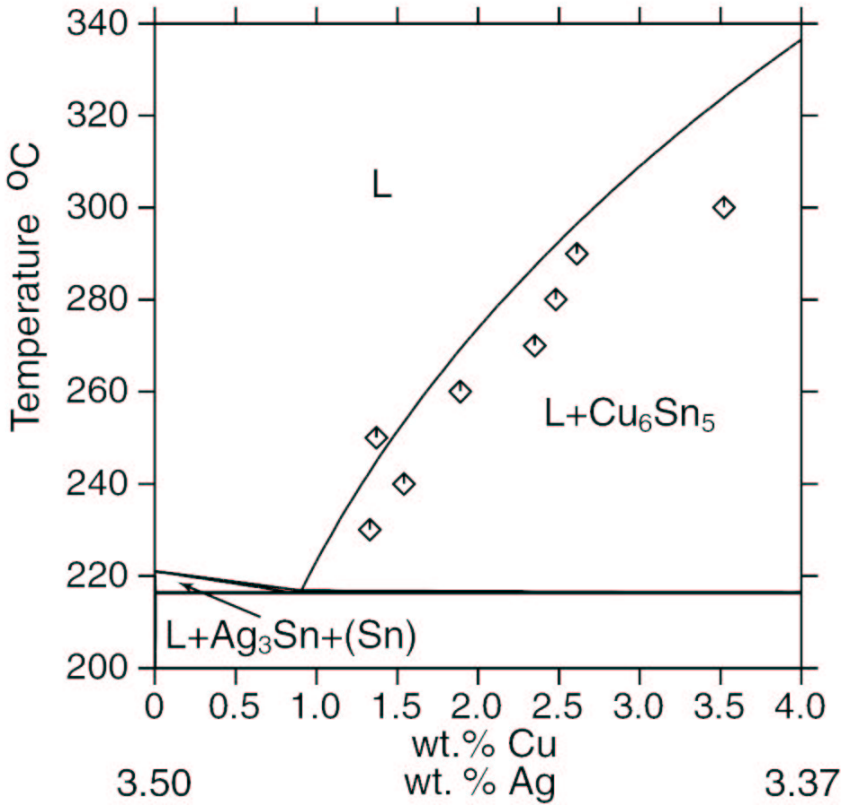

Figure 13. Calculated isopleth between Sn-Ag eutectic in the binary Sn-Ag system and pure Cu with the data of Chada et al. [17]. This plot shows the predicted maximum solubility of Cu in liquid Sn- 3.5 wt % Ag solder as a function of temperature.

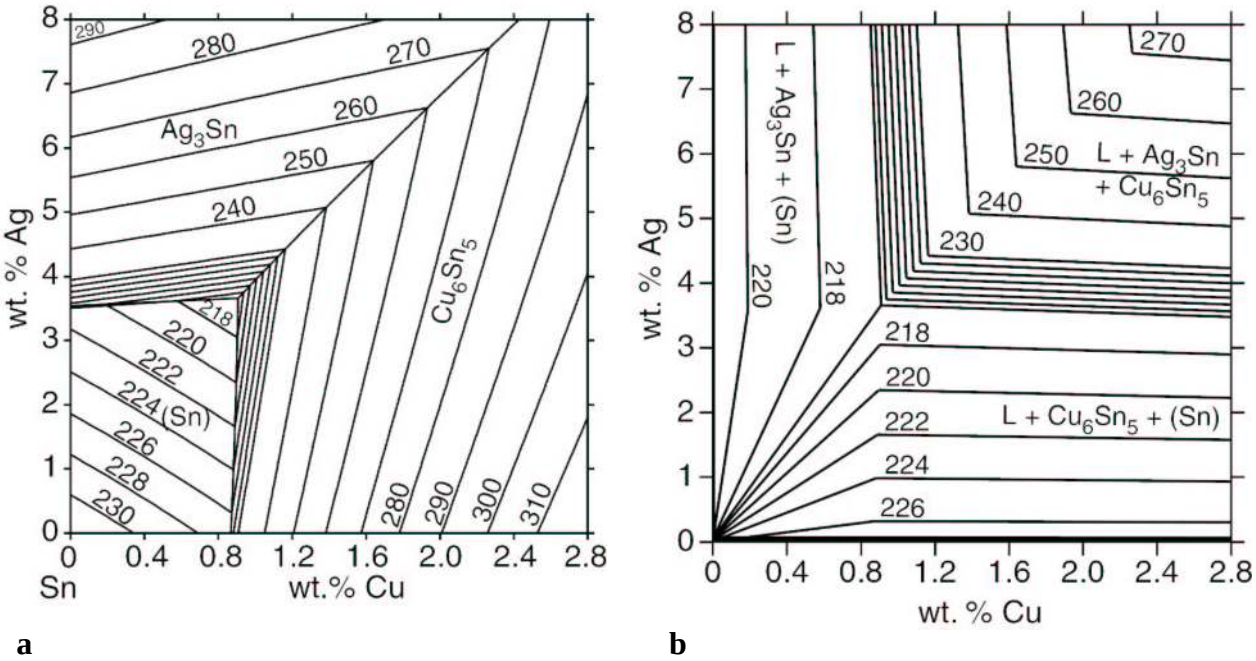

Figure 14. a) Calculated liquidus surface. b) Calculated surface of secondary solidification. Note that the calculated ternary eutectic composition of 3.66 wt % Ag, 0.91 wt % Cu differs from the experimentally determined value of 3.5 wt % Ag, 0.9 wt % Cu.

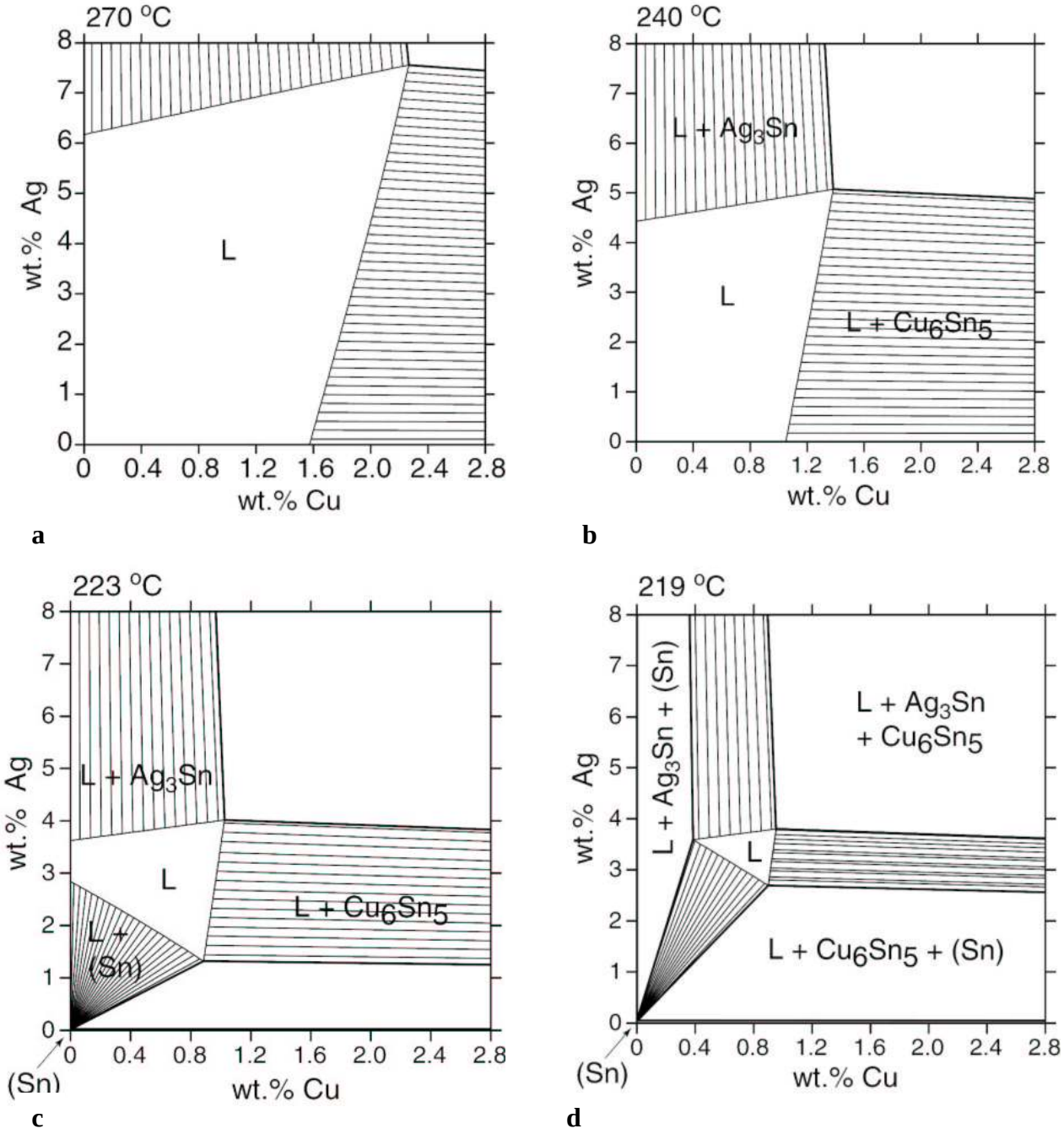

Figure 15. Calculated isothermal sections at a) 270 °C, b) 240 °C, c) 223 °C, and d) 219°C

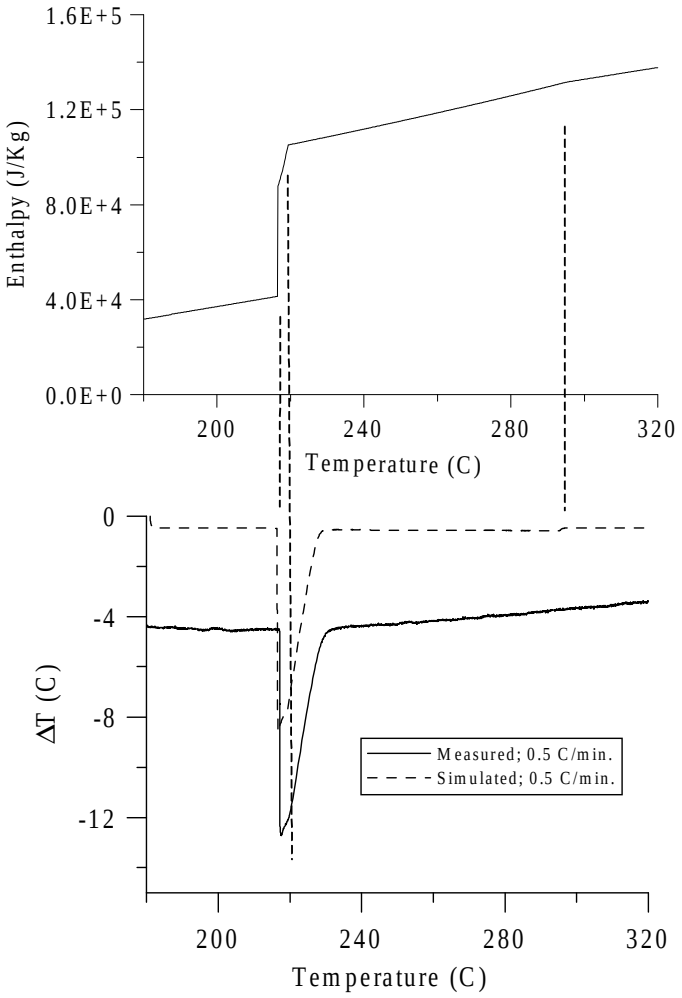

Figure 16. Enthalpy – temperature relationship calculated from thermodynamic Model for Sn-2.3 wt % Cu- 2.5 wt % Ag. Calculated and experimental DTA curves at 0.5 K/min.